UNSTEADY EULER AND NAVIER-STOKES COMPUTATIONS OF A COMPLETE HELICOPTER

T. Renaud, A. Le Pape, C. Benoit
Office National d'Etudes et de Recherches Aérospatiales,
BP 72, 92322 Châtillon Cedex, France

Abstract

The simulation of the aerodynamic interactions between the different parts of a helicopter becomes more and more important for the understanding of the complex flowfield and the design of the helicopter. Advanced numerical tools have been developed in the *elsA* solver in order to represent the various phenomena which occur around the helicopter. Recent progresses have been achieved within the French-German cooperation CHANCE (Complete Helicopter AdvaNced Computational Environment), which aims at the numerical simulation of a complete helicopter. This paper presents results of unsteady Euler and Navier-Stokes computations, using Chimera techniques. The first test-case concerns a Dauphin 365N configuration with its main rotor. A numerical analysis (time convergence, mesh refinement…) allowed to find the best choices for such a complex unsteady simulation. The CFD solutions are in good agreement with measurements done on a Dauphin helicopter model. In the second part, an automatic Cartesian grid approach is applied on a complete configuration (wind tunnel model similar to the NH90 helicopter) in pitch-up flow conditions. The Euler simulation allows to describe the complex flowfield and the interactions between the fuselage and the two rotors.

Notations

p	Pressure, Pa
p_∞	Freestream pressure, Pa
ρ	Density, kg/m^3
ρ_∞	Freestream density, kg/m^3
a_∞	Speed of sound, m/s
R	Blade radius, m
c	Blade reference chord, m
b	Number of blades
r	Spanwise location, m
Re	Reynolds number (based on c and a_∞)
ω	Rotor rotation velocity, rd/s
ψ	Blade azimuth, deg
V_∞	Freestream velocity, m/s
V_r	Blade relative velocity, m/s $V_r = r \cdot \omega + V_\infty \cdot \sin(\Psi)$ for the blades $V_r = V_\infty$ for the fuselage
M_∞	Freestream Mach number
M_{Tip}	Rotor tip Mach number
μ	Advance ratio $\mu = \frac{M_\infty}{M_{Tip}}$
K_p	Pressure coefficient $K_p = \frac{(p - p_\infty)}{\frac{1}{2}\rho_\infty V_r^2}$
T_{Rotor}	Lift force, N
S	Rotor disk area, m^2
σ	Rotor solidity $\sigma = \frac{b \cdot c}{\pi R}$
Z_b	Rotor lift coefficient $Z_b = \frac{100 T_{Rotor}}{\frac{1}{2}\rho(\omega R)^2 S \sigma}$
α	Fuselage incidence angle, deg
Q	Q criteria, s^{-1} $Q = -\frac{1}{2}\frac{\partial V_i}{\partial x_j}\frac{\partial V_j}{\partial x_i}$

Introduction

Due to the inherent complexity of the flowfield around helicopters, advanced tools have to be used in order to represent accurately the various phenomena which occur on the helicopter. At low speed flight or in hover, the main rotor downwash impinges and interacts with the fuselage. The fuselage also modifies the main rotor inflow. Up to now, the design of a new rotorcraft has taken into account this complex interaction by experiments or simple methods. The use of CFD methods can significantly improve the design and solve potential problems early in the program, which is more efficient and less expensive. These CFD models of increasing accuracy have still to be validated by comparing numerical and experimental results.

The rotor-fuselage interactions can be efficiently computed thanks to an actuator disk, which models the rotor by forces discontinuity (Ref. [1], [4]). However, as the pressure jump is time averaged, this leads to a quasi-steady representation of the flowfield.
Thanks to the increase of the computers power, the rotor-fuselage interaction of a complete helicopter can now be simulated by a full unsteady viscous computation (Ref. [2]), although this still remains a challenge in terms of CPU time and disk space storage.
At ONERA, the simulation of rotor/fuselage interactions has been studied for several years by various methods. First, the *PEIRF* code, based on a quasi-steady iterative coupling between two panel methods – one for the rotor and another one for the fuselage – was developed and validated on realistic configurations (Ref. [3]). Actuator disk models have been also used within the new object-oriented Navier-Stokes solver *elsA* (Ref. [4]). Similarly, unsteady simulations of rotating blades have been studied in Euler (Ref. [5]) and Navier-Stokes mode (Ref. [6]). More recently, Ref. [7] demonstrates the capability of the *elsA* solver to simulate the interactions between a wind tunnel model support and a helicopter rotor with soft blades in a weak coupling process. This last computation and the configurations presented in this paper were part of the final objective of the French-German cooperation CHANCE (Complete Helicopter AdvaNced Computational Environment). This program aimed at developing and validating CFD methods allowing the simulation of unsteady viscous flows around a complete helicopter.
This paper deals with the unsteady Euler and Navier-Stokes simulations of complete helicopter configurations. At first, the numerical methods, in particular the Chimera approach, are briefly presented. A Dauphin 365N fuselage configuration with its main rotor has been simulated. In particular, a time convergence study and a comparison with the experimental database (steady and unsteady pressures, PIV measurements) are discussed. In the second part of this paper, another Chimera strategy with automatic Cartesian grid generation has been applied on a wind tunnel model configuration similar to the NH90 helicopter with its main and tail rotors. The aerodynamic flow and the interactions between the fuselage and the two rotors are described based on qualitative results.

Numerical method

ElsA solver

ONERA has started in 1996 the unification of his different aerodynamic solvers in an unique object-oriented code, *elsA* (Ensemble Logiciel de Simulation en Aérodynamique). It is based on multiblock structured meshes where Reynolds averaged Navier-Stokes equations in a finite volume formulation allow to simulate a large variety of applied configurations (aircraft, turbomachinery, helicopters …). In the framework of the CHANCE program, new specific developments have been realized in the *elsA* solver, in particular for the Chimera method.
For the present computations, the velocity of the infinite state is equal to zero and body motions – translation for the fuselage and translation + rotation for the blades - are applied. The 2^{nd} order spatial discretisation of the conservative system is ensured by the space-centred Jameson's scheme. The 2^{nd} and 4^{th} order coefficients of the Jameson artificial viscosity are equal respectively to 0.5 and 0.016. The time integration is done with the backward Euler scheme and an LU scalar relaxation implicit phase. A sub-iterative Newton-like method resolves the time Gear equations and allows to accelerate the convergence by the use of large azimuthal steps. For the Navier-Stokes computations, the k-ω turbulence model is used with the SST correction and the Zheng limiter. The calculations do not include any transition criteria.

Chimera technique

The Chimera method allows to simplify the meshing process for complex geometries and relative moving bodies. It consists in overlapping child grids on background ones and transfers of the different solutions thanks to interpolation algorithm. The solution of the child grids is transferred to the background grid thanks to masks (holes in the background mesh where the solution is transferred) around the bodies. For Navier-Stokes computations, in order to avoid perturbations in important gradient areas (viscous layers…) due to the interpolation algorithm, the masks are located some cells far from the wall surfaces. In the *elsA* software, several methods of interpolation are available (Ref. [8]): the cell search procedure like the ICG method (interpolation Cartesian grid) for unsteady flows or the ADT method (alternating digital tree) for steady flows. Similarly, different shapes can be used for the blanking process: Cartesian, cylindrical…

Dauphin 365N configuration

This test-case concerns the Dauphin 365N helicopter model in the following flow conditions: freestream velocity V_∞=15m/s (M_∞=0.044, advance ratio μ=0.15), Reynolds number Re=1.07 10^6 m^{-1} and angle of incidence α=-3°. The rotor thrust coefficient is Z_b=14.5. This 1/7.7 scaled powered model has been intensively tested in the S2Ch wind tunnel during the 90's and more recently in the F1 wind tunnel (Ref. [9]). The main characteristics of the Dauphin powered model are the following:

- Fuselage length L_{fus}=1.5m
- Rotor radius R=0.75m
- Blade root cutout R_{cut}=0.206m
- Blade chord c=0.05m (constant)
- Rotor solidity σ=0.0849
- Blade tip velocity ΩR=100m/s

The control angles values were obtained from a HOST simulation (HOST is the Eurocopter comprehensive code for the flight mechanics) of the isolated rotor of the Dauphin model. This means that the rotor trim does not account the rotor-fuselage interactions. The rotor thrust delivered by HOST is Z_b=14.765. The blades are assumed to be rigid, which is a reasonable approximation in the present case. Other test cases aiming at demonstrating the capability of *elsA* to perform unsteady viscous simulations with soft blades are presented in Ref. [7].

The Chimera method is required here for overlapping the blades grids on the helicopter fuselage grid:

- Background grid: the mesh around the D365N fuselage has been constructed at ONERA with the *ICEM-CFD* software. The CAD geometry has been simplified (fenestron removed, simplification of the engines fairing geometry, no modelization of the strut and of the rotor hub). The finest grid has a total of about 7.4 million points distributed in 97 blocks. A coarser grid has been obtained by taking one another point in all directions and has a total of about 0.9 million points. This coarse grid has been used also for the Euler computations. Figure 1 shows a general view of the grid, specifying the fuselage and the rotor positions.
- Child grid: a C-H child grid envelops each blade. The Euler grid contains 141x59x25 points (~832.000 points for the 4 blades). About 100 points are distributed on each airfoil surface and 30 sections in the spanwise direction. The Navier-Stokes grid (Figure 2) contains 181x57x41 points (~1.7 million points for the 4 blades). About 120 points are distributed on each airfoil surface and 30 sections in the spanwise direction.

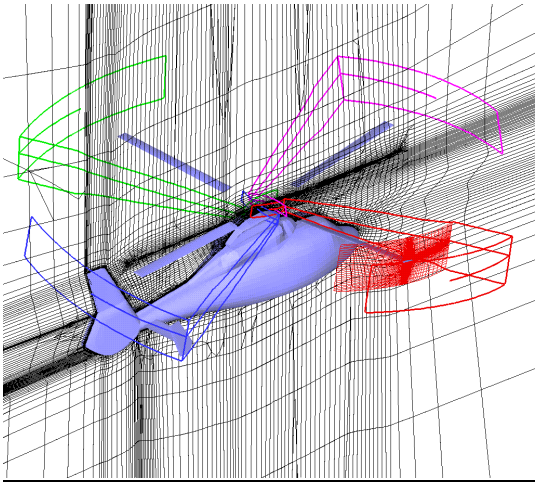

Figure 1 - Background grid around the Dauphin 365N fuselage

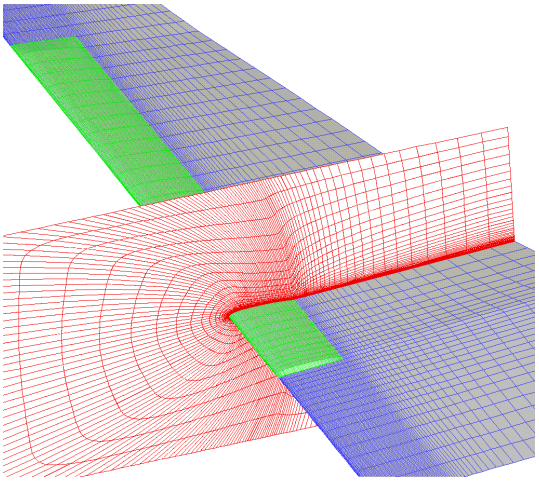

Figure 2 - Navier-Stokes blade grid

Euler/Navier-Stokes comparison

Euler and Navier-Stokes computations have been performed on the fuselage coarse grid during 3 rotor revolutions in order to get a satisfying convergence of the solutions. The chosen physical timestep corresponds to 0.6° per iteration. For each timestep, 15 Gear sub-iterations are computed with a LU implicit phase and a backward-Euler time integration. This allows to converge the sub-iterations with a decrease of the residuals by approximately 2 orders at each time step. The Euler and the Navier-Stokes calculations require respectively 45 hours and 66 hours CPU time for one rotor revolution on a NEC SX6.

As seen on Figure 3 and Figure 4, the different non-dimensioned fluxes are well periodic at the end of the computations. Figure 3 presents the convergence history of the fuselage lift force. The curves show high frequency oscillations, probably due to the lack of preconditioning for those computations at low speed. The development of the preconditioning method in a rotating frame in the *elsA* solver is in progress. The viscous effect of the Navier-Stokes computation seems to decrease slightly the oscillations. Additionally, the low frequency oscillation amplitude of the lift is also reduced. Viscous calculations provide a smaller mean lift force than the Euler calculation. Figure 4 presents the convergence history of the non-dimensioned rotor lift force (Z_b). The periodicity of the oscillations after 3 rotor revolutions shows the good convergence of the computation. The differences between the Euler and Navier-Stokes solutions are more significant for the rotor loads than for the fuselage loads (the Euler and the Navier-Stokes blade grids are not the same). The mean lift value changes from Z_b=14.2 for the Euler solution to Z_b=13 for Navier-Stokes. Even if the rotor lift resulting from the Euler simulation is closer to experiment than the Navier-Stokes rotor lift, only a weak coupling procedure similar to that used in Ref. [7] could provide a truly trimmed and fully representative CFD solution.

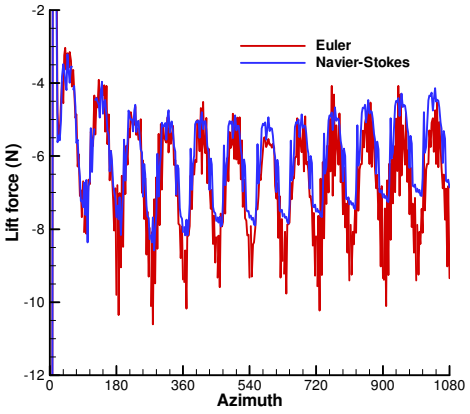

Figure 3 - Convergence histories of the fuselage lift force

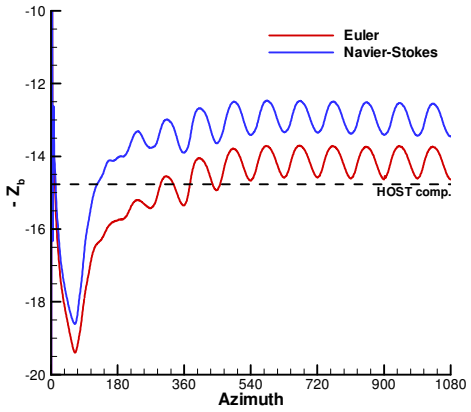

Figure 4 - Convergence histories of the rotor thrust coefficient

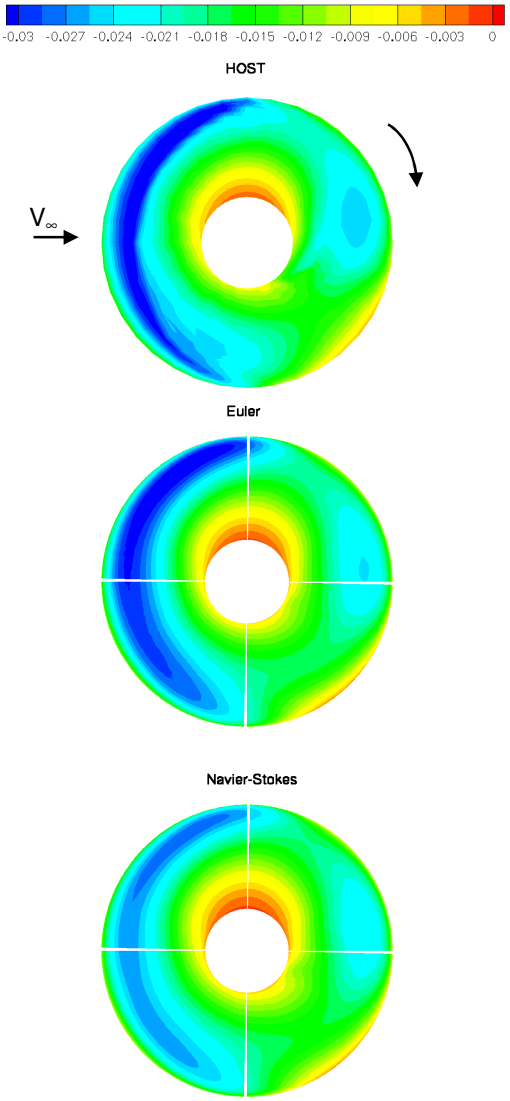

Figure 5 - Comparison of the sectional lift coefficients (C_nM^2) between elsA Euler and Navier-Stokes computations and HOST results

Figure 5 presents a comparison between the *elsA* computations (CFD Euler and Navier-Stokes methods) and the HOST results, concerning the sectional lift coefficient $C_N M^2$. Note the negative values of the $C_N M^2$ corresponding to a lifting rotor, due to the sense of rotation and coordinate system used for the present simulation. Figure 5 shows the lift coefficient distribution on the rotor disk. The numerical simulations all give a correct estimation of the lift distribution. As seen before, the Euler solution is in better agreement with the HOST result with higher levels of thrust. The viscous effects tend to decrease the lift in the front area of the rotor ($90° < \Psi < 270°$).

Time convergence

A time convergence study has been performed on the coarse grid using the Gear time integration. Figure 6 presents the time convergence history of the rotor thrust and Figure 7 the time convergence history of the sectional lift at r/R=0.97. For each figure, the effects of the number of sub-iterations and of the physical time step are plotted. A third graph compares the evolutions for a same total number of iterations (constant value of sub-iterations/$\Delta\Psi$ = 40 iter/°). A reference solution (black curves) is chosen with ($\Delta\Psi$, subiter) = (1°, 80).

It is obvious that increasing the number of sub-iterations or decreasing the physical timestep allows to improve the solution convergence but it is important to find a compromise in order to avoid a too high CPU time consumption. The solutions corresponding to ($\Delta\Psi$, subiter) = (1°, 10) and ($\Delta\Psi$, subiter) = (1°, 20) are quite different from the solutions given by ($\Delta\Psi$, subiter) = (1°, 40) and ($\Delta\Psi$, subiter) = (1°, 80), which are very close (top of Figure 6 Figure 7). In the present calculations and methods, 40 sub-iterations correspond to a mean global residual reduction of 3 orders.

In the second set of analyses, the solution with ($\Delta\Psi$, subiter) = (0.5°, 20) compares well with the reference solution ($\Delta\Psi$, subiter) = (1°, 80), whereas a timestep of $\Delta\Psi$=2° does not allow to capture the phase and the amplitude of the aerodynamic phenomena (middle of Figure 6 Figure 7). The third set of graphs confirms this conclusion, even if the number of sub-iterations is increased up to 80 (in particular on the rotor thrust evolution). The parameters ($\Delta\Psi$, subiter) = (0.5°, 20), ($\Delta\Psi$, subiter) = (1°, 40) and ($\Delta\Psi$, subiter) = (1°, 80) provide very similar results. However, as shown in Table 1, the CPU time cost per rotor revolution (obtained on a NEC SX6 processor) is higher for the smallest physical timestep. It is essentially due to the Chimera extrapolation research which is performed at each timestep and not during sub-iterations. Then, the best compromise seems here to be the solution given by ($\Delta\Psi$, subiter) = (1°, 40).

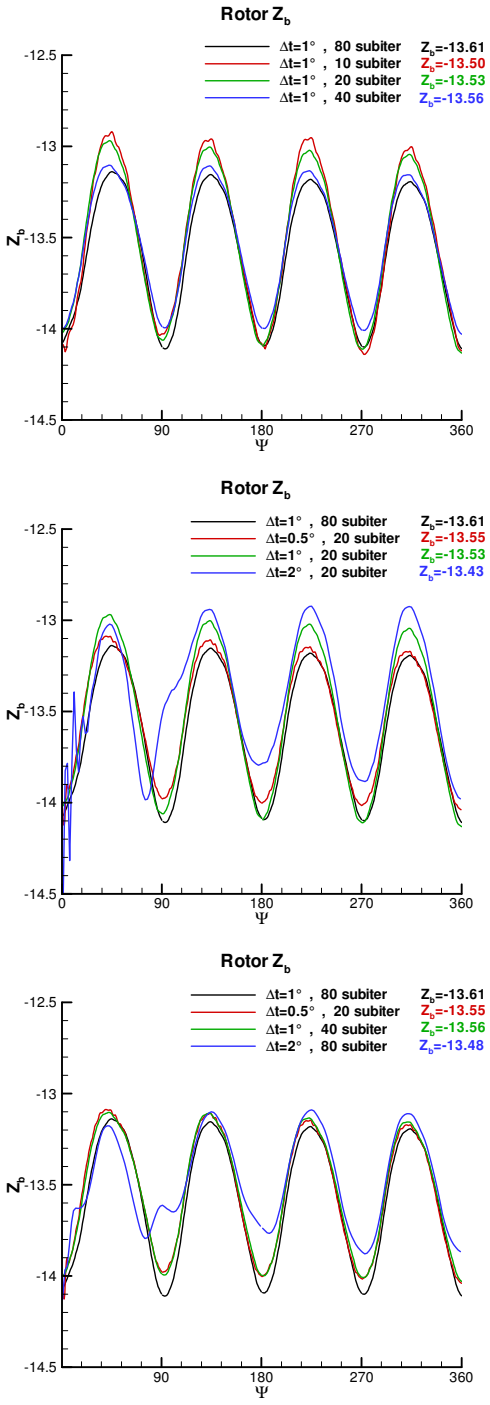

Figure 6 - Time convergence history of the rotor thrust

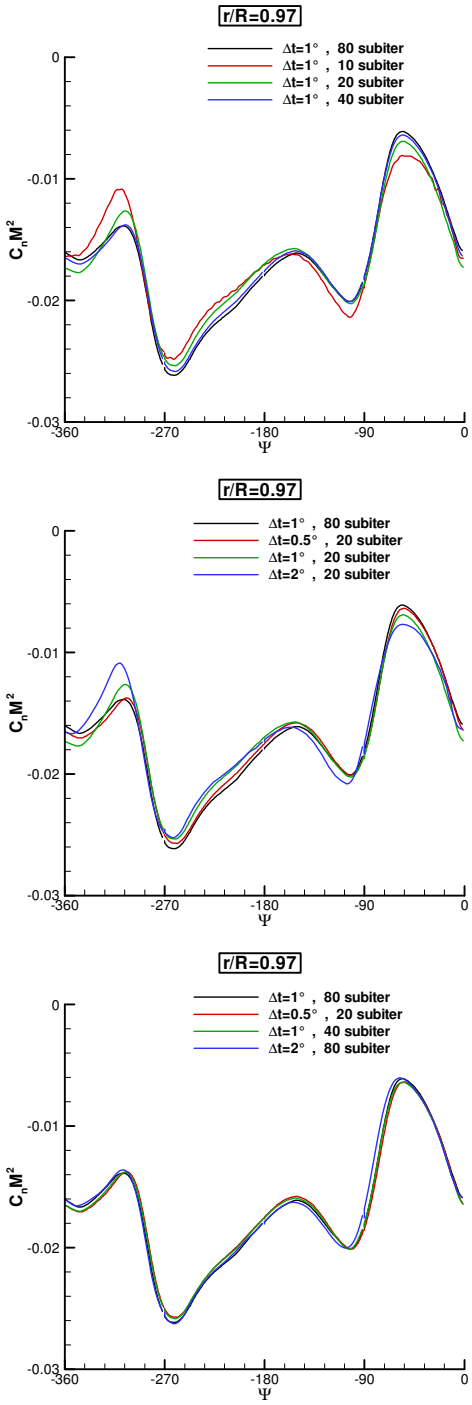

Figure 7 - Time convergence of the sectional lift coefficient at r/R=0.97

Table 1 – CPU cost comparison for the time convergence study

ΔΨ	Subiter.	CPU time per rotor revolution
1°	80	320.113s
0.5°	20	310.039s
1°	40	229.484s
2°	80	152.077s

Effect of the mesh refinement

The effect of the mesh refinement has been analyzed by taking the fine fuselage grid. The global mesh size is about 9 million points. According to the previous conclusions, a computation has been performed using (ΔΨ, subiter) = (1°, 40). The CPU time cost on a NEC SX6 processor is 508.413s per rotor revolution. As before, a correct convergence of the solution is obtained after 3 rotor revolutions.

Figure 8 presents a comparison of the fuselage forces evolutions between the coarse and the fine mesh solutions. The numerical results are also compared to the experimental values, which have been obtained thanks to an uncoupled balance system during the S2Ch wind tunnel campaign. Even if the low Mach number preconditioning has not been applied on the fine mesh simulation, the 3 forces evolutions show less high frequency oscillations with the finest grid. Moreover, the mesh refinement improves clearly the loads results. The mean values of the drag and the lift are in better agreement with the S2Ch experiment. However, no improvement is observed concerning the side force.

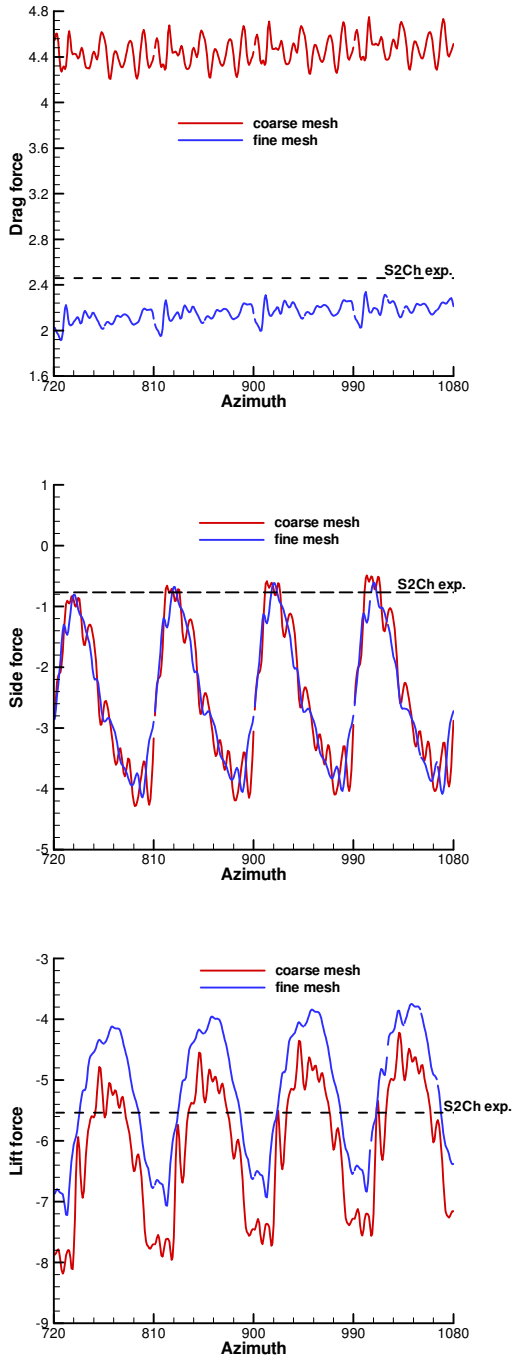

Figure 8 - Effect of the mesh refinement on the fuselage loads evolutions

In the mesh refinement analysis, only the fuselage grid has been changed. However, Figure 9 shows that this affects also significantly the rotor solution. Indeed, the rotor thrust is decreased with the finest mesh by about 2%. An enrichment of the harmonic content of the rotor thrust evolution can be noticed for the fine grid solution: the decreasing phase of $|Z_b|$ is faster than the increasing phase.

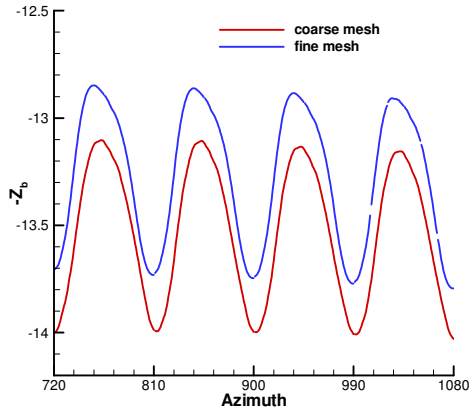

Figure 9 - Effect of the mesh refinement on the rotor thrust evolution

Comparison with pressure measurements

Figure 10 presents the pressure coefficient (K_P) distribution along the upper centerline of the fuselage. The unsteady pressure values have been averaged during one period (90°). There are few differences between the coarse and the fine grids curves, apart the smoothing of the solution with the finest mesh. The numerical averaged results are then in good agreement with the experimental steady pressure values. It may be also interesting to compare the averaged solution of an unsteady computation with the quasi-steady solution obtained with an actuator disk modelling. As seen on Figure 10, both approaches provide close results (the actuator disk computation has been realized with a low Mach number preconditioning and so it does not reveal such big numerical oscillations), but of course, the actuator disk approach is largely cheaper in CPU time (factor of 15). However, the unsteady simulations allow to obtain frequencies of the aerodynamic phenomena or real wake structures, as shown in the next part.

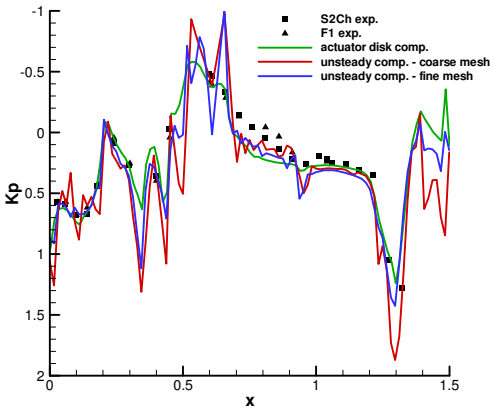

Figure 10 - Comparison between unsteady and actuator disk computations

Figure 11 shows the unsteady pressure coefficient evolutions and the FFT analysis for the transducers 4 and 27 located along the upper centerline respectively on the nose and the tail boom of the fuselage. As said before, the numerical results, in particular on the fuselage, show high frequency oscillations due to the lack of preconditioning in these low speed flight conditions. The mesh refinement tends to smooth slightly those oscillations. The rotor-fuselage interaction is noticeable by the 4/rev component of the signals, due to the four blades passage. The experimental results, as well as the numerical solutions, reveal that the intensity of the rotor/fuselage interaction (higher value of ΔK_p) is more important at transducer 27, i.e. on the tail boom, than on the nose of the fuselage.

These numerical results are in very good agreement with the experiment. The CFD simulations slightly underestimate the FFT values for transducer 4. The fine grid solution improves the accuracy for the transducer 27. The 4/rev harmonic corresponds to the passage of the four blades, but the 8/rev mode seems to be also important in the rotor/fuselage interaction. At transducer 27 where the rotor/fuselage interaction is the strongest, the 4/rev and 8/rev FFT values are increased by comparison with transducer 4, located on the nose of the fuselage.

Comparison with the PIV measurements

Figure 12 and Figure 13 present slices of the computed flowfield with coarse and fine meshes The first one is a comparison concerning the iso-contours of the Y-vorticity component in the retreating blade side (Y=0.5). The mesh refinement allows to capture more than one vortex core in the blade wake (blue vortices) with respect to the coarse grid solution. The successive vortex sheets are also better represented and are in good agreement with the experimental view. In the front part of the rotor, the wake is better resolved with the fine grid. Indeed, the different vortex paths tend to collapse together when the numerical diffusion is too important.

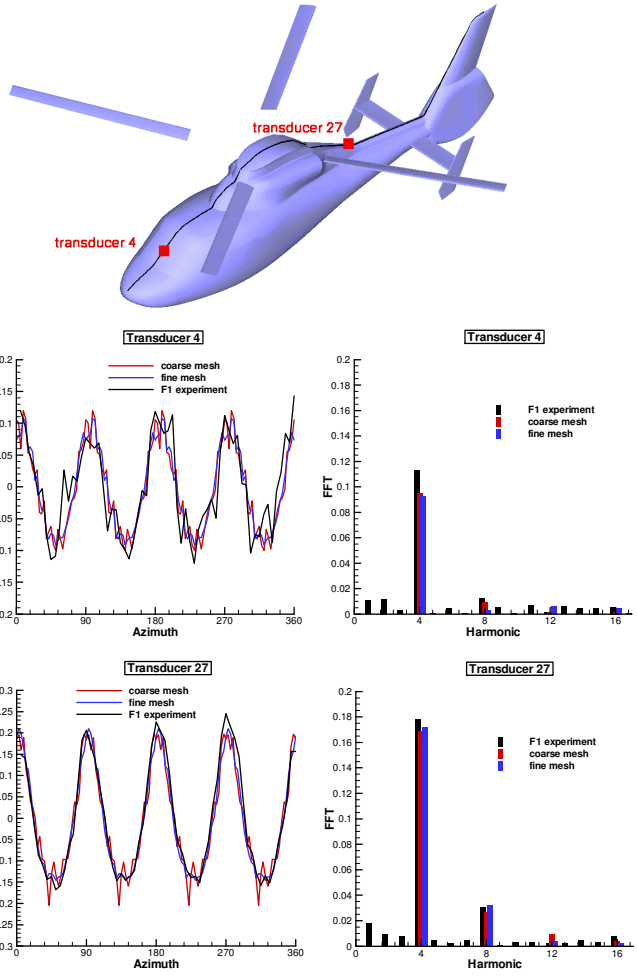

Figure 11 - Unsteady pressure coefficient and FFT comparisons for transducers 4 and 27

Figure 13 concerns the iso-contours of the streamwise vorticity just aft of the fuselage (X=1.5175). The computational results are compared to experimental PIV measurements (Ref. [9]). The CFD simulation is able to capture the main vortices, such as the two tip vortices and the fuselage wake. For the coarse mesh solution, the position of the vorticity area near the left empennage is quite well represented by the calculation, but the left tip vortex (advancing side) is predicted too low compared to the blade. The effect of the mesh refinement is here

significant. The two tip vortices are better captured and located compared to the experimental PIV visualization. Moreover, some small structures in the rotor wake are also captured, in particular the successive vortices and vortex sheets coming from the different blades just above the left vertical empennage. The fuselage wake near the right vertical empennage is only captured by the fine mesh, in agreement the experimental solution. Of course, a finer mesh is still requested to improve the CFD solution, in particular in the rotor wake, far from the fuselage body. But it could also be interesting to apply other numerical methods, such as a higher order spatial scheme or the vorticity confinement approach (Ref. [10]) for a more accurate capturing of the wake structure.

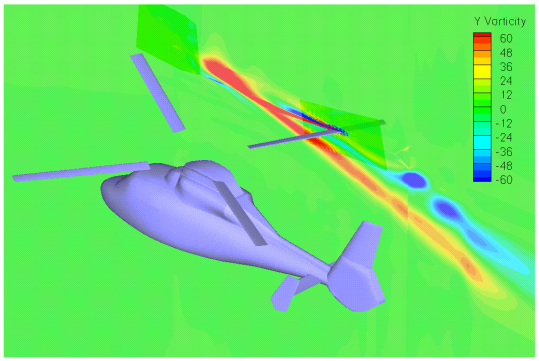

Navier-Stokes coarse mesh

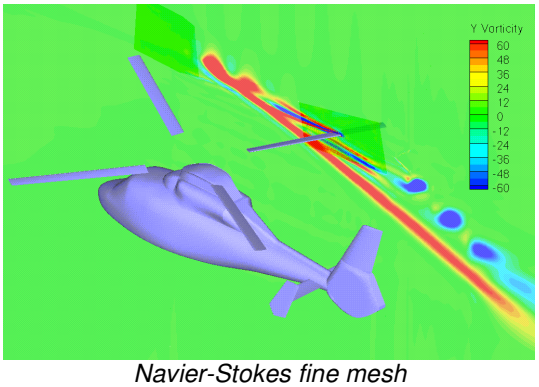

Navier-Stokes fine mesh

Figure 12 - Computational iso-contours of vorticity for the retreating blade side

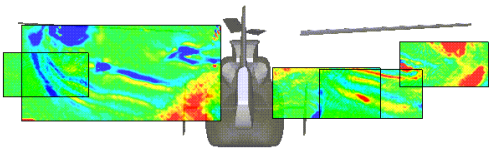

F1 experimental PIV measurements

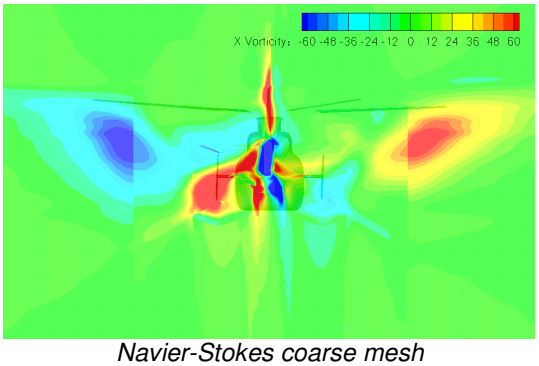

Navier-Stokes coarse mesh

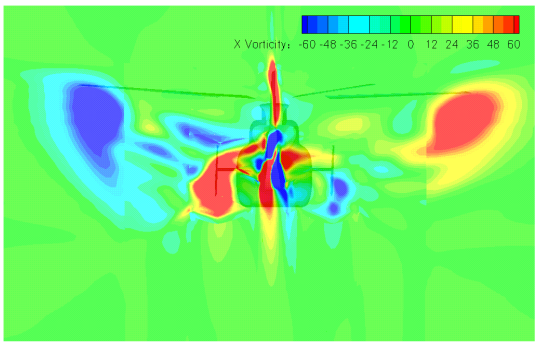

Navier-Stokes fine mesh

Figure 13 - Experimental and computational iso-contours of streamwise vorticity just aft of the fuselage

NH90 wind tunnel model configuration

This test-case concerns a wind tunnel model similar to the NH90 helicopter with its main and tail rotors in the following flow conditions: freestream velocity V_∞=13.9m/s (M_∞=0.041, advance ratio μ=0.064) and angle of incidence α=7.08°. Those conditions correspond to a helicopter pitch-up configuration. The control angles values of the main rotor have been provided by Eurocopter. Only a collective pitch angle is applied on the tail rotor blades.

The automatic Cartesian mesh generation (Ref. [11]) is an alternative strategy to the basic Chimera approach used for the Dauphin 365N configuration. It involves also the Chimera technique but the background grid is composed

by Cartesian blocks automatically generated by the solver. These blocks are refined in the vicinity of the child grids. Moreover, this strategy allows to automatically adapt the background grid, avoiding some problems in the interpolation cells research. Thus, for the present NH90 configuration, the mesh contains 4.56 million points composed as follows:

- *Background grid*: a composite Cartesian mesh automatically created by the *elsA* solver (in black in Figure 14). The 174 blocks of this mesh are matched each other with a "patched grid" boundary condition. The minimum size of the cells is found to be coherent with the mean size of the external layer of all the child grids. This mesh contains about 2.17 million points.
- *Child grids*:
  - *Fuselage grid*: the near-body grid around the NH90 fuselage contains 125 blocks and about 1 million points.
  - *Main rotor grid*: the Navier-Stokes mesh of the rotor blade contains 153x57x35 points (i.e. 1.22 million points for the 4 blades). 100 points are distributed on the airfoil surface and 30 in the spanwise direction.
  - *Tail rotor grid*: the mesh of the tail rotor grid contains 157x55x37 points. The mesh is coarsened by taking only one another point (i.e. about 168.000 points for the 4 blades).

The blades are assumed to be rigid. This test case aims at demonstrating the capability of the *elsA* solver to perform a complete helicopter computation with an automatic Cartesian grid strategy and thus a simple Euler calculation has been performed. The Newton like method (20 Gear sub-iterations) is applied for a timestep Ψ=1°. A main rotor revolution requested 180 hours CPU time on a Dec Alpha 833MHz processor.

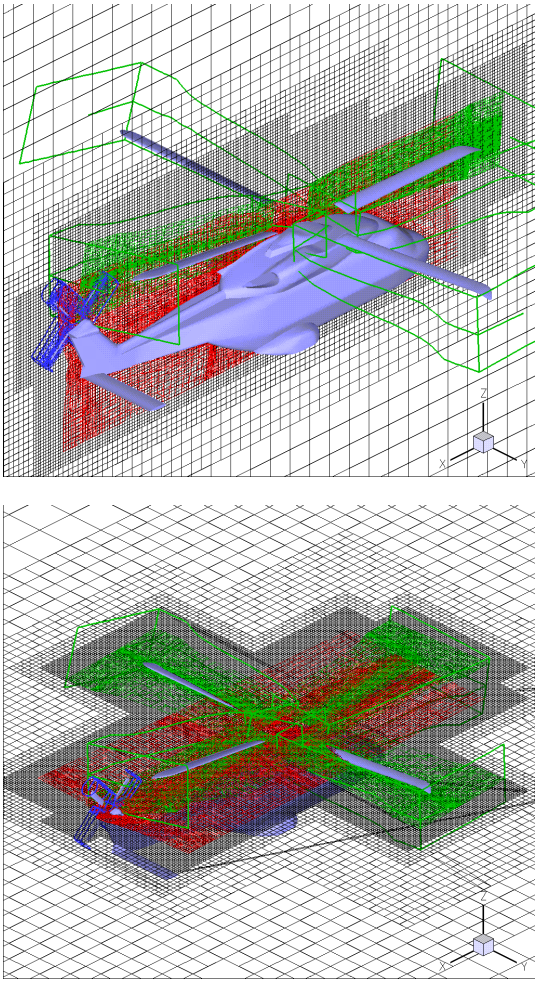

Figure 14 - 3D meshes visualizations for the automatic Cartesian grid strategy

Figure 15 shows the history of the non-dimensioned main rotor thrust Z_b which tends to stabilize until Ψ=540°: the computed Z_b is close to 11.5. This value underestimates the HOST rotor thrust coefficient Z_b=13.5. With respect to the previous Dauphin configuration where the lift evolution revealed the 4/rev frequency due to the 4 blades passage, Figure 15 shows also a 8/rev harmonic which can be due to the effect of the tail rotor on the main rotor. However, this interaction probably increases the time to obtain a well converged solution. This is confirmed by Figure 16, where the sectional lift coefficient is plotted at r/R=0.975 during the last rotor revolution of the computation. The main discrepancies between the 4 blades take place in the rear part of the rotor (Ψ~0°), where the interaction with the flow induced by the tail rotor is the most significant.

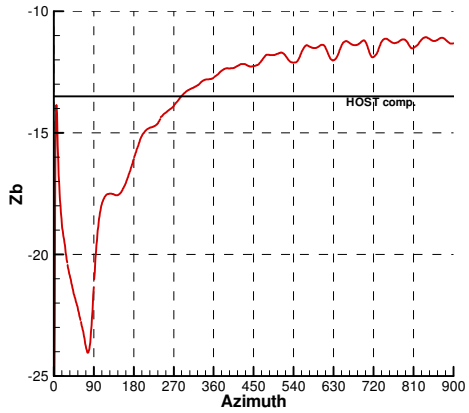

Figure 15 - Convergence of the main rotor thrust

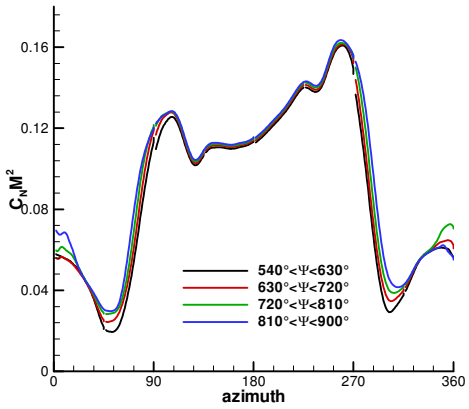

Figure 16 - Sectional lift coefficient at r/R=0.975

In Figure 17, the contour levels of Mach number are presented in the tail rotor plane. For such low speed flow conditions, the streamlines are strongly deflected by the main rotor thrust. The main rotor wake appears clearly where the flow is accelerated in the rear part of the fuselage and it strongly interacts with the tail rotor. The clockwise tail rotor slows down the upper part of the wake and the streamlines are slightly deflected to the top. In the other side of the helicopter, the main rotor wake will interact with the horizontal empennage and lead to the pitch-up phenomenon.

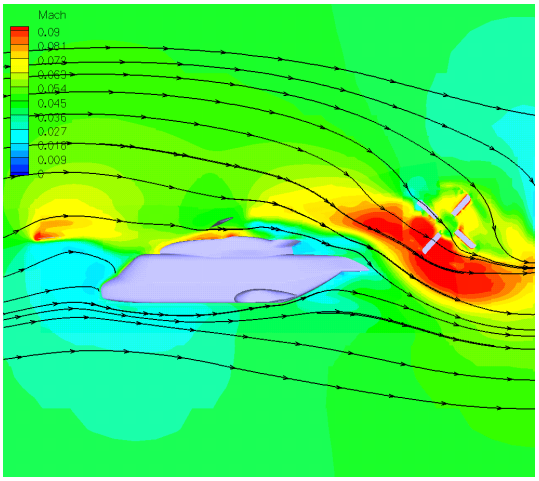

Figure 17 – Iso-contours of Mach number in the tail rotor plane

In Figure 18, an iso-surface of the Q criteria is colored by the X-component of the vorticity. The fine mesh allows a satisfying capture of the blade vortex paths in the proximity of the bodies, but the right and left blade tip vortices begin to be lost due to the numerical dissipation in a coarser mesh area. An interaction between the main and tail rotors is predicted and the iso-surface of vorticity around the tail rotor impacts the different main rotor vortex paths. It appears that the tail rotor tends to deviate and to drift the two blade tip vortices induced by the main rotor wake. Other parts of the body seem to create strong vorticity, such as the nose, the sponsons and the horizontal stabilizer.

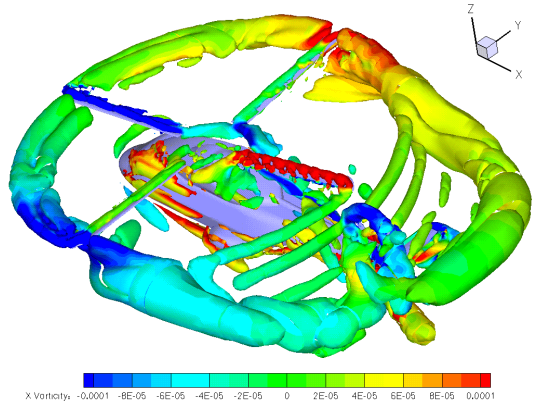

Figure 18 – Iso-surface of Q criteria colored by the X-component of vorticity

Figure 19 presents the instantaneous pressure distribution on the fuselage and the blades. This instant shows the front blade moving from the right and the rear blade from the left of the fuselage. The pressure repartition is then

asymmetric. In particular, the left engine exhaust and the left side of the tail boom are more impacted than the right one. In contrary, the right side of the fuselage nose reveals higher pressure coefficient values. This figure shows also the effect of the tail rotor downwash on the vertical fin. It can also be noticed that a large zone of negative pressure on the nose side is calculated (blue levels). This corresponds to large separation area on both sides of the fuselage nose due to the large fuselage incidence, as seen with the iso-surface of Q criteria in Figure 18.

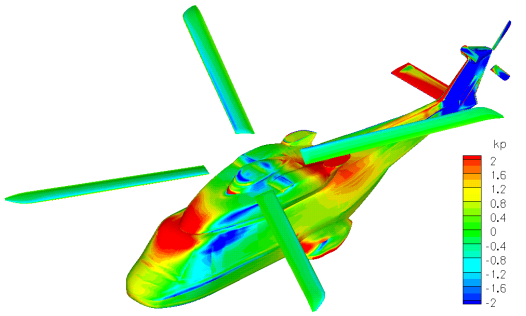

Figure 19 – Iso-contours of pressure coefficient

Conclusion

Computations of two complete helicopter configurations have been presented in this paper. At first, a numerical study (Euler/Navier-Stokes comparison, time convergence, mesh refinement) has been performed on the Dauphin 365N fuselage with its main rotor. This simulation allows explaining the mechanisms of the rotor/fuselage interaction and shows a satisfying comparison with the F1 experimental database. The unsteady pressure evolutions are in very good agreement with the experimental results on various transducers locations, both in amplitude and phase. The fine mesh is able to capture accurately the blade vortices and to compare well with the PIV measurements.
The second test-case concerned a wind tunnel model similar to the NH90 helicopter with its main and tail rotors. It was the first simulation on such a complex geometry and it demonstrates the ability of the *elsA* code to compute a complete helicopter. In particular, an original mesh strategy has been applied, consisting in overlapping body grids (fuselage, main rotor blades and tail rotor blades) on a Cartesian background grid, which was automatically generated by an *elsA* functionality. It allowed reducing the interpolation problems of the Chimera method, when parts are added to an existing mesh. An Euler simulation allowed to describe features of the flowfield and the strong interactions between the fuselage with its two rotors. The absence of experimental data for this NH90 test-case does not allow to confirm the validity of this analysis. However, this first simulation will help in short terms for a comparison between computations and for example the GoAhead experimental database within an on-going European program.
In the future, the effort has to be put on the computational time reduction of such complex configurations, in particular with the use of parallel computers. The perspective of this work will also be the improvement of the rotor wakes. Of course, finer meshes are still requested to improve the CFD solution but it can also be interesting to apply other numerical methods, such as a higher order spatial scheme or the vorticity confinement approach. These numerical developments are planned in the framework of the SHANEL French-German project and will be applied to study other specific helicopter problems (tail-shake, blade vortex interaction …).

Acknowledgements

The authors would like to acknowledge the French Ministry of Transport DPAC and Ministry of Defence SPAé for the financial support of the numerical studies presented in this paper.
The authors are thankful to NHIndustries and Eurocopter for providing the NH90 wind tunnel model data.

References

[1] F. Le Chuiton
Actuator disk modeling for helicopter rotors
28th European Rotorcraft Forum, Bristol, UK, September 2002

[2] M. Potsdam
Dynamic rotorcraft applications using overset grids
31st European Rotorcraft Forum, Florence, Italy, September 2005

[3] D. Gasser, N. Bettschart, B. Drouin
Theoretical and experimental studies on unsteady helicopter rotor-fuselage interactional aerodynamics
American Helicopter Society, Vertical Lift Aircraft Design Conference, San Francisco, CA, January 1995

[4] T. Renaud, C. Benoit, J.-C. Boniface, P. Gardarein
Navier-Stokes computations of a complete helicopter configuration accounting for main and tail rotors effects
29th European Rotorcraft forum, Friedrichshafen, September 2003

[5] J. C. Boniface, P. Guillen, M. C. Le Pape, D. Darracq, P. Beaumier
Development of a Chimera unsteady method for the numerical simulation of rotorcraft flowfields
36th Aerospace Sciences Meeting & Exhibit, Reno, NV, January 1998

[6] P. Beaumier, J.-M. Bousquet
Applied CFD for analysing aerodynamic flows around helicopters
ICAS 2004, Yokohama, Japan, August/September 2004

[7] B. Rodriguez, C. Benoit, P. Gardarein
Unsteady computations of the flowfield around a helicopter rotor with model support
AIAA Paper 2005-466

[8] C. Benoit, M.-C. Le Pape, G. Jeanfaivre
Improvement of the robustness of the Chimera method
32nd AIAA Fluid Dynamics Conference & Exhibit, Saint-Louis, USA, June 2002

[9] A. Le Pape, J. Gatard, J.-C. Monnier
Experimental investigations of rotor-fuselage interactions using a helicopter powered model
30th European Rotorcraft Forum, Marseilles, France, September 2004

[10] Y. Wenren, J. Steinhoff
Application of vorticity confinement to the prediction of the wake of helicopter rotors and complex bodies
17th Applied Aerodynamics Conference, Norfolk, USA, June 1999

[11] C. Benoit, G. Jeanfaivre
3D inviscid isolated rotor and fuselage calculations using Chimera and automatic Cartesian partitioning methods
Journal of the American Helicopter Society, pp. 128-138, April 2003